A New Hill Climbing Maximum Power Tracking Control for Wind Turbines with Inertial Effect Compensation

Murat Karabacak, Luis M. Fernández Ramírez, *Senior Member, IEEE*, Tariq Kamal, *Student Member, IEEE*, and Shyam Kamal, *Member, IEEE*

***Abstract*— Finding and tracking maximum power point are two important dynamics in the control of variable speed wind turbines, since they determine the efficiency of wind turbines. The conventional hill climbing possesses the problems of wrong directionality and low performance, since it does not take the inertial effect into account. In this study, a novel hill climbing method is proposed by considering the inertial effect to solve these problems. Besides, employing the exact model knowledge of the generator in the maximum power tracking control deteriorates the efficiency considerably, therefore it is required to design a parameter independent and robust control system if possible. Thus, the third order super twisting sliding mode and continuous integral sliding mode controllers are designed for the control of generator and grid side converters to track the maximum power trajectory accurately, and they are compared to each other for the chattering in experimental results. A comparison is also performed between the conventional and proposed hill climbing methods based on the captured energy from the wind. Experimental results, with a wind turbine emulator, demonstrate that the proposed hill climbing method relaxes the wrong directionality and sluggish performance of the conventional one.**

***Index Terms*—Wind energy, Higher order sliding mode Control, Integral sliding mode control, Hill climbing**

I. INTRODUCTION

Owing to the intermittent characteristic of wind, maximum power tracking is an imperative requirement to increase the efficiency of the wind turbines. To this aim, Variable Speed Wind Turbines (VSWTs) have been developed to increase the efficiency in comparison with constant speed wind turbines [1]. Maximum Power Point Tracking (MPPT) is achieved by adapting the turbine speed optimally below rated wind speed. Two important dynamics arise when the MPPT based control of VSWTs is the subject, these are the instantaneous detection and tracking of the Maximum Power Point (MPP). In the literature, there are widely used MPPT methods based on Generator Signal Feedback (GSF), Tip Speed Ratio (TSR), Optimal Torque Control (OTC), Wind Turbine Power Curves (WTPC) and Hill Climbing (HC) [47].

GSF and OTC based MPPT methods use the exact model knowledge of the generator as a priori, especially the torque constant. TSR based MPPT method employs, as a priori, the exact model knowledge of the turbine, coming from the parameters of the swept area of the blades and the air density [47]. Furthermore, TSR and WTPC necessitate using an anemometer on the contrary to GSF and OTC. WTPC control also requires real test data, which it is difficult to get. All those methods, GSF, OTC, TSR, and WTPC cause a wrong detection of MPP at some level, thus the turbine efficiency decreases to a lower level [2]-[4]. HC searching MPPT control is popularly used in photovoltaics energy systems, which requires neither turbine nor generator parameters, and it needs no wind sensor in wind turbines, as well. However, the conventional HC method does not consider the energy stored in the turbine inertia, and thus the problems of wrong directionality and low convergence speed arise. To cope with these problems, a new HC searching MPPT control method is proposed by considering the inertial energy in this study, which makes it possible to detect the MPP accurately even under rapid wind variations [47].

The conventional HC fails to follow the MPP trajectory under rapid wind variations. Furthermore, sudden wind variations may also lead to the unstable operation of the wind turbine [5]-[9]. Consequently, the conventional HC method is not effective for particularly large-inertia wind turbine systems, since the generator output power is greatly influenced by the change rate of the rotor inertial energy in the transient. In the conventional HC method, small step sizes lead to slow convergence speeds, and large step sizes lead to oscillations around MPP, for small-inertia turbines. An additional issue called wrong directionality appears for particularly large-inertia turbines [2], [10]-[13]. It is required to utilize a low pass filter for filtering the inertial power component of the generator output power, and to properly tune the cut-off frequency of it. All these actions result in a certain degrade in precise detection

Manuscript received September 02, 2018; November 28, 2018; February 11, 2019; accepted February 27, 2019.

This study is supported by the Scientific and Technological Research Council of Turkey (TUBITAK) Research Fund (Project No. 114E159), the authors thank to the TUBITAK.

M. Karabacak is with the Department of Electrical and Electronics Engineering, Sakarya University of Applied Sciences, Sakarya, 54187, Turkey (e-mail: muratkarabacak@sakarya.edu.tr).

T. Kamal is with the Department of Electrical and Electronics Engineering, Sakarya University, Sakarya/Serdivan, 54187, Turkey (e-mail: tariq.kamal.pk@ieee.org).

L. M. Fernández-Ramírez and T. Kamal are with the Research Group in Electrical Technologies for Sustainable and Renewable Energy (PAIDI-TEP-023), Department of Electrical Engineering, Higher Polytechnic School of Algeciras, University of Cadiz, 11202 Algeciras, Spain (e-mail: tariq.kamal.pk@ieee.org; luis.fernandez@uca.es).

S. Kamal is with Department of Electrical Engineering, Indian Institute of Technology, Varanasi, Uttar Pradesh, 221005, India (email: shyamkamal.eee@iitbhu.ac.in).

of MPP and lead to an efficiency decrement [14]-[15], [47].

In the literature, there is no study conducted about HC method and its derivatives to eliminate the inertial effect. However, there are several papers [6], [14]-[21] that studied how the wrong directionality problem can be overcome and the efficiency increases. It was stated in [6] that there is a need for an online training process, which requires a large amount of memory, and reliability problems may occur. A combination of OTC and hill climb search was proposed in [14]. However, it presents the problems, mentioned above, related to OTC. A derivative of hill climb search method was presented in [15], which needed a wind sensor. A method was implemented in [16] by using the exact model knowledge of the turbine. As mentioned above, using the exact model knowledge causes the efficiency to decrease to lower levels. In [17]-[19], a DC link voltage slope was used in MPPT control to avoid the wrong directionality problem. These methods require a relatively low DC link voltage control bandwidth to allow slopes to easily occur during wind speed changes, which causes large DC link voltage deviations under rapid wind changes. This means that there is an unwanted reactive power interaction between wind turbine and grid. In [20], a method requiring a priori knowledge, was evaluated. An adaptive filter with the fuzzy logic hill climbing control criterion without an experimental validation was analyzed in [21]. Simulation results were satisfactory, but a complex scheme was used. Consequently, the conventional HC has a tradeoff between the convergence speed and the turbine efficiency due to the inertial effect [14], [15], [17]-[19].

To obtain high performance by eliminating this trade-off, in this study, a new inertial-power based HC is proposed without compromising the convergence speed and the turbine efficiency. Thus, the proposed HC based MPPT control method avoids the wrong directionality problem, existed in the conventional HC method, under sudden wind speed changes. The proposed HC method uses the generator speed and the turbine input power as inputs, although the conventional one uses the generator speed and the generator output power. This method is especially important for the MPPT control of wind turbines with large inertia. For high efficiency, instantaneously tracking MPP is also essential and this requires a controller robust against parameter and external disturbance uncertainties. Fixed gain linear controllers do not show strong robustness against parameters and external disturbance variations [22]-[24]. In addition, fuzzy and artificial intelligence based MPPT methods were also presented in the literature [25]-[28], but their applications in the wind energy industry were seldom recorded. Many authors have stated that the sliding mode control approach is more robust with respect to matched uncertainties [29]-[32]. Nevertheless, chattering is the main limitation of sliding mode control. To address this issue, the higher order sliding mode was developed [33]. The higher order of sliding increases the robustness against uncertainties and reduces chattering [34], [47].

In this paper, a third order super-twisting and continuous integral sliding mode controllers are separately designed for the control of generator and grid side converters, where no prior knowledge of parameters is used. It must be noted that these controllers are feasible and comparable, since both of their control inputs are continuous in time. Consequently, the conventional and proposed HC methods are separately implemented with both the third order and integral sliding mode control methods. Finally, the conventional and proposed HC methods are compared in terms of the MPPT efficiency.

II. Wind Turbine Configuration

A PMSG wind turbine was considered in this work. The wind turbine was emulated by an induction motor using the model described as follows:

$$T_{in} = P_{in}/\omega_r = C_p P_w/\omega_r = 0.5\rho\pi R^5 C_p\left(\omega_r^2/\lambda^3\right) - J_r\dot{\omega}_r \qquad (1)$$

$$P_{in} = C_p P_w = 0.5 C_p \rho A V^3 - J_r \omega_r \dot{\omega}_r \qquad (2)$$

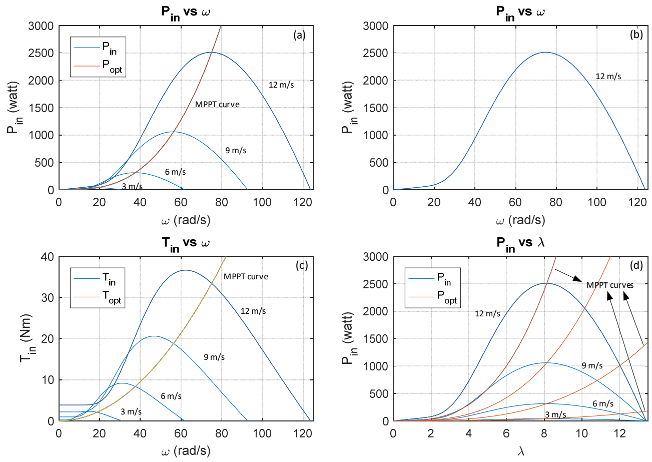

Fig. 1. Wind turbine response for wind speeds of 3, 6, 9 and 12 m/s: (a), (b) P_{in} *vs* ω; (c) T_{in} vs ω; and (d) P_{in} *vs* λ

$$C_p(\lambda,\beta) = c_1\left(c_2/\lambda_i - c_3\beta - c_4\right)e^{(-c_5/\lambda_i)} + c_6\lambda \qquad (3)$$

$$1/\lambda_i = 1/(\lambda + 0.08\beta) - 0.035/(\beta^3 + 1) \qquad (4)$$

where P_{in} and T_{in} are the turbine input power and torque, respectively; C_p is the turbine power coefficient; J_r is the turbine inertia; ω_r is the turbine speed; A is the swept area of the turbine rotor; λ is the tip speed ratio; and β is the pitch angle, which is assumed to be zero in this study because the wind turbine is emulated at below rated wind speed.. The wind turbine parameters and coefficients used in Eqs. (1)-(4) are given in Appendix [35]. The inputs of the emulator are the wind speed, wind rotor inertia, and generator speed. The output is the turbine input torque. The characteristic curves of the wind turbine considered in this work are given in Fig. 1 for wind speeds of 3, 6, 9 and 12 m/s. From Fig. 1, the optimum value of the tip speed ratio and the power coefficient are 8.129 and 0.48, respectively. For the rated wind speed (12 m/s), the optimum speed and torque of the turbine rotor are 75 rad/s and 33.39 Nm, respectively. A virtual gear with $N = ¾$ conversion ratio is used to obtain, with the emulator, 100 rad/s and 25 Nm as rated speed and torque, and thus, a rated power of 2.5 kW for the emulated wind turbine.

Fig. 2 shows the scheme of the complete experimental setup for the wind turbine considered in this work. The wind turbine emulator implements the turbine model shown in Fig. 2. An induction motor with rotor field-oriented control is used to emulate the wind turbine. More information about the rotor field-oriented control implemented in this work can be found in [36]. One TMS320F28335 board is used for the control of the power converters associated to the wind turbine emulator and

This article has been accepted for publication in a future issue of this journal, but has not been fully edited. Content may change prior to final publication. Citation information: DOI 10.1109/TIE.2019.2907510, IEEE Transactions on Industrial Electronics

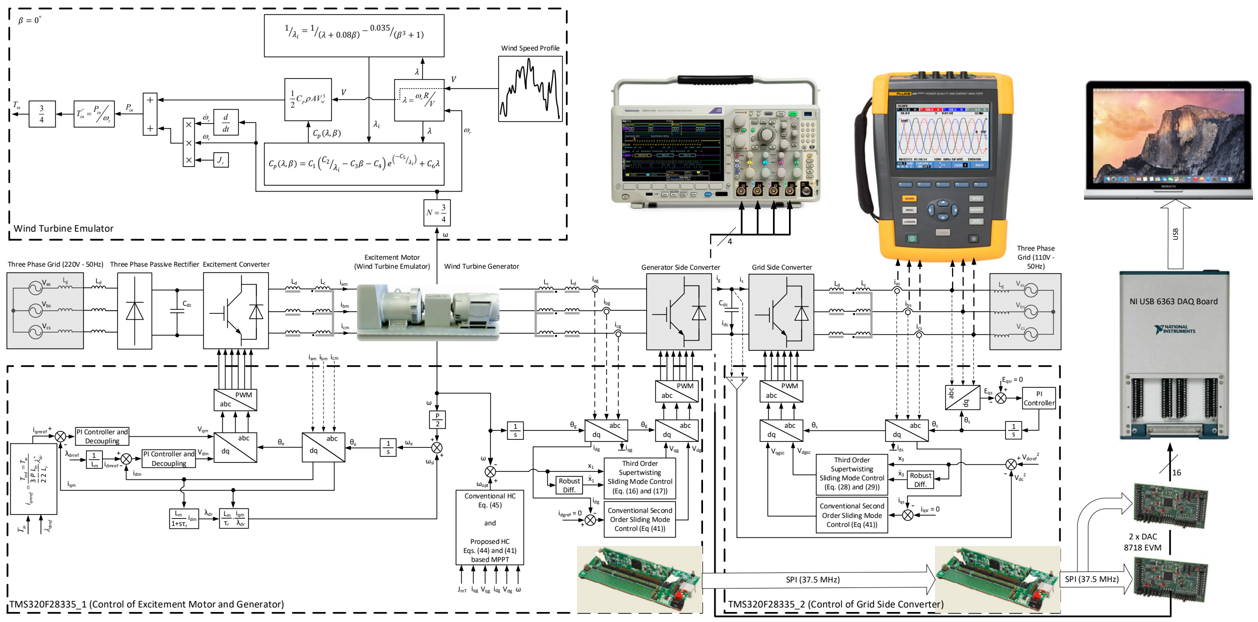

Fig. 2. Scheme of the complete experimental setup for the wind turbine

the generator side converter, and the other board is used for the control of the grid side converter.

III. Proposed Control System with the Higher Order Super-Twisting Sliding Mode Control

The higher order super twisting sliding mode controller is proposed for those systems having a relative degree more than one. The main advantage of this controller is the chattering reduction, since it produces a continuous control signal. Perturbations must be Lipschitz continuous, that is, the first derivatives need to exist almost everywhere and be bounded, which is necessary condition for the asymptotic stability [37]-[39]. With the aim of obtaining a strong robustness against model and external disturbance uncertainties, and ensuring a high tracking performance of MPP, the Third Order Super-Twisting Sliding Mode Control (TOSSMC) is applied to the control of generator and grid side inverter.

A. Third Order Super-Twisting Sliding Mode Controller for PMSG

The PMSG used in this work has a very low salience effect, so it is assumed as a surface magnet machine, thus the *d*-axis desired current i_{dgref} is set to zero [22], [23], [40]. The dynamic equations of PMSG in the synchronous reference frame are given by [22], [23]:

$$V_{dg} = R_s i_{dg} + L_{dg}\, di_{dg}/dt - \omega_g L_{qg} i_{qg} \tag{5}$$

$$V_{qg} = R_s i_{qg} + L_{qg}\, di_{qg}/dt + \omega_g L_{dg} i_{dg} + \omega_g \lambda_m \tag{6}$$

$$d\omega/dt = \left(1/J_g\right)\left(T_g - T_{in}\right) \tag{7}$$

$$T_g = \left(3P/2\right)\lambda_m i_{qg} \tag{8}$$

The *d*-axis current i_{dg} is set to zero for maximum torque per ampere. V_{qg} and V_{dg} are the control inputs on *q*- and *d*- axis respectively, ω_g is the generator electrical speed, and T_g is the generator electromagnetic torque. For the control of the PMSG, the speed tracking error is firstly defined as:

$$\begin{aligned} x_1 &= \omega_{opt} - \omega \\ x_2 &= i_{qg} \end{aligned} \tag{9}$$

Taking derivative of Eq. (9) and using Eq. (7), it is obtained:

$$\dot{x}_1 = -\left(3P\lambda_m/2J\right)\left(x_2 + f_1\right) \tag{10}$$

$$f_1 = -\left(2J/3P\lambda_m\right)\dot{\omega}_{opt} - \left(2/3P\lambda_m\right)T_L \tag{11}$$

Using Eq. (6), it follows:

$$\dot{x}_2 = \left(V_{qg} + f_2\right)/L_{qg} \tag{12}$$

$$f_2 = -R_s x_2 - \omega_g L_{dg} i_{dg} - \omega_g \lambda_m \tag{13}$$

where f_1 and f_2 are matched nonvanishing disturbance. Although the system resulting from Eq. (10) and (12) has a relative degree two concerning x_1, it is not possible to apply higher order sliding mode directly because the system is not in chain of integrator form. To this aim, the following changes are further required to achieve the chain of integrator form [47]:

$$\dot{x}_1 = z_1 \tag{14}$$

$$\dot{z}_1 = -\left(\frac{3P\lambda_m}{2JL_{qg}}\right)V_{qg} - \left(\frac{3P\lambda_m}{2JL_{qg}}\right)f_2 - \left(\frac{3P\lambda_m}{2J}\right)\dot{f}_1 \tag{15}$$

Then, the TOSSMC control law is given by Eq. (16) and (17) [37], [38]. Detailed information about the general stability analysis can be found in [41].

$$\phi_1 = \dot{x}_1 + k_2 \left|x_1\right|^{2/3} sign\left(x_1\right) \tag{16}$$

$$V_{qg} = k_1 \left|\phi\right|^{1/2} sign\left(\phi\right) + k_3 \int_0^t sign\left(\phi\right) d\tau \tag{17}$$

where k_1, k_2, and k_3 are positive finite control gains.

Remark 1. For selecting gains above, in general, the Lyapunov based trial-and-error method, which was taken from [41], is used. This fact is also valid for the control of the grid side converter explained in Section B.

Remark 2. It is important to note here that the information of z_1 cannot be used to design the control input V_{qg} because it contains information of f_1. Therefore, it is need for the robust exact differentiator to calculate $\dot{x}_1$.

B. Third Order Sliding Mode Controller for the Grid Side Converter

There are various control methods for grid side converters. Voltage oriented control is the most important control scheme, since it is applicable to many industrial fields such as wind and solar energy conversion systems, uninterruptable power supplies and active power filters, among others. Dynamic equations of the grid side converter are given by [42], [47]:

$$V_{dgsc} = R_d i_{ds} + L_d \, di_{ds}/dt - \omega_s L_q i_{qs} + V_{ds} \tag{18}$$

$$V_{qgsc} = R_d i_{qs} + L_q \, di_{qs}/dt + \omega_s L_d i_{ds} + V_{qs} \tag{19}$$

$$dV_{dc}^2/dt = \left(3V_{ds}/2C_{dc}\right) i_{ds} - \left(1/C_{dc}\right) V_{dc} i_g \tag{20}$$

where i_g represents the external disturbance to the control system, V_{dgsc} and V_{qgsc} are the control inputs, V_{ds} and V_{qs} are the grid voltages, i_{ds} is the d-axis current, set to zero for zero reactive power, and i_{qs} is the q-axis current. Eq. (20) is obtained by neglecting the convertor losses, under the synchronism conditions [43]. The grid synchronism angle is obtained by the synchronous PLL, which can provide a high performance because of balanced grid in effect. Appropriately, for the control of grid side converter, the DC bus voltage tracking error is firstly defined as:

$$x_3 = V_{dcref}^2 - V_{dc}^2;\ x_4 = i_{ds} \tag{21}$$

where the output is V_{dc}^2. Using Eq. (20), the derivative of Eq. (21) takes the form of:

$$\dot{x}_3 = -\left(3V_{ds}/2C_{dc}\right)\left(x_4 + f_3\right) \tag{22}$$

$$f_3 = -\left(4C_{dc}/3V_{ds}\right) V_{dcref} \dot{V}_{dcref} + \left(2/3V_{ds}\right) V_{dc} i_g \tag{23}$$

The d-axis current tracking error and its derivative, by using Eq. (18), are given by:

$$\dot{x}_4 = \left(V_{dgsc} + f_4\right)/L_s \tag{24}$$

$$f_4 = -R_s i_{ds} + \omega_s L_s i_{qs} - V_{ds} \tag{25}$$

where f_3 and f_4 are matched nonvanishing disturbance. The system composed of Eqs. (22) and (24) has a relative degree two case. However, as in the previous case, to design TOSSMC, the following changes are made:

$$\dot{x}_3 = z_3 \tag{26}$$

$$\dot{z}_3 = -\left(\frac{3V_{ds}}{2C_{dc}L_s}\right) V_{dgsc} - \left(\frac{3V_{ds}}{2C_{dc}L_s}\right) f_4 - \left(\frac{3V_{ds}}{2C_{dc}}\right) \dot{f}_3 \tag{27}$$

Then, the TOSSMC control law is given by Eqs. (28) and (29) [37]-[38].

$$\phi_3 = \dot{x}_3 + k_5 \left|x_3\right|^{2/3} sign\left(x_3\right) \tag{28}$$

$$V_{dgsc} = k_4 \left|\phi\right|^{1/2} sign\left(\phi\right) + k_6 \int_0^t sign\left(\phi\right) d\tau \tag{29}$$

where k_4, k_5, and k_6 are positive control gains. For the general stability analysis, one can refer to the reference in [41].

Remark 3. It is important to note here that the information of z_3 cannot be used to design control input, V_{dgsc}, because it contains the information of f_3. Therefore, there is need for the robust exact differentiator to calculate $\dot{x}_3$.

Conventional Super-Twisting Controller (STC) is employed in the d axis current control of generator and in the q axis current control of grid side converter [44]. To reveal the real time implementation of TOSSMC and STC, detailed schemes are given in Fig. 3 and Fig. 4 respectively.

C. Continuous Integral Sliding Mode Control for PMSG

First, the sliding manifold is described below for the relative degree two system given in Eqs. (14) and (15) as:

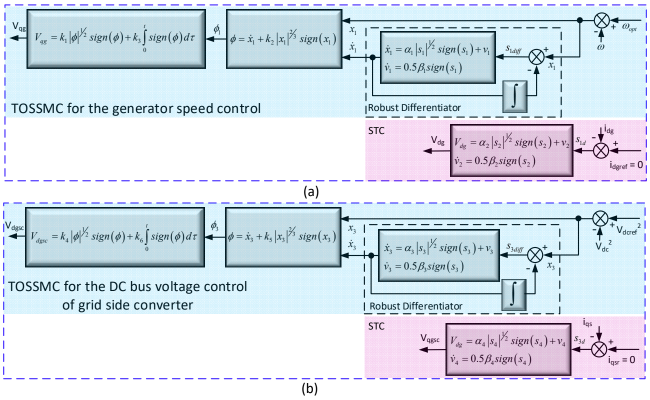

Fig. 3. Control loops of the wind turbine: (a) TOSSMC and STC for the generator; (b) TOSSMC and STC for the grid side converter.

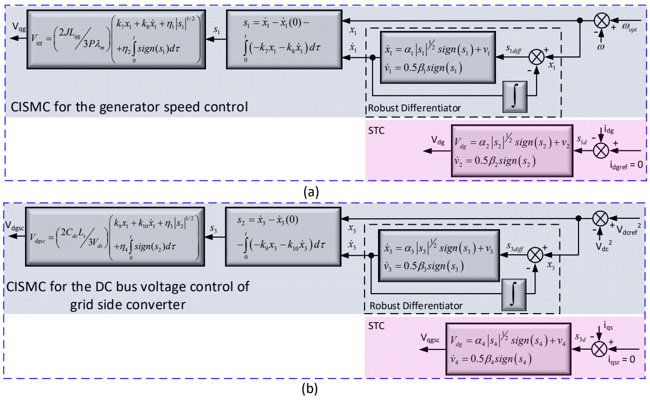

Fig. 4. Control loops of the wind turbine: (a) CISMC and STC for the generator; (b) CISMC and STC for the grid side converter.

$$s_1 = \dot{x}_1 - \dot{x}_1(0) - \int_0^t \left(-k_7 x_1 - k_8 \dot{x}_1\right) d\tau \tag{30}$$

where $\dot{x}_1(0)$ is the initial value, its value is considered zero here. Differentiating Eq. (30) yields:

$$\dot{s}_1 = -\left(\frac{3P\lambda_m}{2JL_{qg}}\right)\left(V_{qg} + f_2\right) - \left(\frac{3P\lambda_m}{2J}\right) \dot{f}_1 + k_7 x_1 + k_8 \dot{x}_1 \tag{31}$$

Control law of Continuous Integral Sliding Mode Control (CISMC) is designed below to ensure that $\dot{s}_1 = 0$ as:

$$V_{qg} = \left(\frac{2JL_{qg}}{3P\lambda_m}\right)\left(k_7 x_1 + k_8 \dot{x}_1 + \eta_1 \left|s_1\right|^{1/2} + \eta_2 \int_0^t sign(s_1) d\tau\right) \tag{32}$$

The resulting dynamics of the sliding manifold is obtained below by inserting Eq. (32) in Eq. (31):

$$\dot{s}_1 = -\eta_1 \left|s\right|^{1/2} - \eta_2 \int_0^t sign(s) d\tau + \xi\left(f_2, \dot{f}_1\right) \tag{33}$$

where $\xi(f_2, \dot{f}_1) = -(3P\lambda_m/2JL_{qg})f_2 - (3P\lambda_m/2J)\dot{f}_1$. Since Eq. (33) stands for the STC algorithm, $\eta_1 > 1.41(\eta_2 + \dot{\xi})^{1/2}, \eta_2 > \dot{\xi}$, and hence $(s_1, \dot{s}_1) \to (0,0)$ as $t \to \infty$. Therefore, from the initial point onwards, it can be concluded that $\eta_2 \int_0^t sign(s) d\tau = -\xi(f_2, \dot{f}_1)$. Substituting the control law of Eq. (32) into the closed loop system in Eqs. (14) and (15) produces the following differential equation.

$$\dot{x}_1 = z_1$$

$$\dot{z}_1 = -k_7 x_1 - k_8 \dot{x}_1$$

(34)

where it is possible to prove that $x_1 \to 0$ and $z_1 \to 0$ as $t \to \infty$ from the eigenvalues analysis of the closed loop linear homogeneous system given by Eq. (34), which means the closed loop system is globally asymptotically stable [46].

D. Continuous Integral Sliding Mode Control for the Grid Side Converter

Sliding manifold is defined below for the relative degree two system given in Eqs. (26) and (27).

$$s_3 = \dot{x}_3 - \dot{x}_3(0) - \int_0^t \left(-k_9 x_3 - k_{10}\dot{x}_3\right) d\tau \tag{35}$$

where $\dot{x}_3(0)$ is the initial value, which equals to zero. Control law based on CISMC is designed below to ensure that $\dot{s}_3 = 0$ as:

$$V_{dgsc} = \left(\frac{2C_{dc}L_s}{3V_{ds}}\right)\left(k_9 x_1 + k_{10}\dot{x}_1 + \eta_3 |s_2|^{1/2} + \eta_4 \int_0^t sign(s_2) d\tau\right) \tag{36}$$

Substituting the control law of Eq. (36) into the closed loop system produces the following differential equation, which governs the closed loop systems as:

$$\begin{aligned} \dot{x}_3 &= z_3 \\ \dot{z}_3 &= -k_9 x_3 - k_{10}\dot{x}_3 \end{aligned} \tag{37}$$

It is obvious that the closed loop system is globally asymptotically stable, exactly as in the previous case [46].

E. Robust Differentiator for the Sliding Mode Controllers and the Proposed HC Method

A robust differentiator is designed to take the time derivative of x_1 and x_3 [44], [45]. Without loss of generality, it is assumed that the input signal is measurable, and it consists of a base signal having a derivative with Lipschitz's constant, $C > 0$. An auxiliary function is described to differentiate x_1 and x_3 as:

$$\dot{x} = u \tag{38}$$

The following sliding surface can be defined as:

$$s = x - x_k(t) \ldots k = 1,3 \tag{39}$$

Differentiating s leads to the following relationship:

$$\dot{s} = u - \dot{x}_k \tag{40}$$

The super-twisting control law below can be thus described as [44], [45].

$$\begin{aligned} u &= \dot{x}_k = \alpha_k |s|^{1/2} sign(s) + v \\ \dot{v} &= 0.5\beta_k sign(s) \end{aligned} \tag{41}$$

where $\alpha_k > C$ and $\beta_k > 4C\,(\alpha_k + C)/(\alpha_k - C)$ or $\alpha_k > 1.1C$ and $\beta_k > \sqrt{C}$, all of them are positive finite control gains, and u gives the $\dot{x}_k$. Detailed information can be found in [45].

IV. Conventional and Proposed Inertial Power based HC Methods

In the proposed HC, $\Delta P_{in}/\Delta\omega$ & $\Delta P_g/\Delta\omega$ are evaluated under the certain conditions, as seen from Fig. 6. However, only $\Delta P_g/\Delta\omega$ is evaluated in the conventional HC, as seen from Fig. 5. This implies that the energy stored in inertia is neglected in the conventional one, which makes the conventional HC blind to wind speed changes [14], [15].

A. Proposed HC Method for the MPPT Control

The proposed HC method is presented in Fig. 6. In this method, only the total inertia of the turbine at the generator side, $J_{mT} = J_m + J_g + J_r N^2$, is used as a priori knowledge.

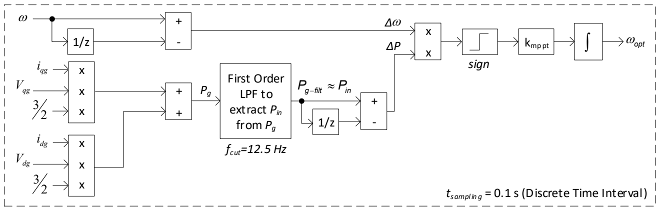

Fig. 5. The conventional HC based MPPT method

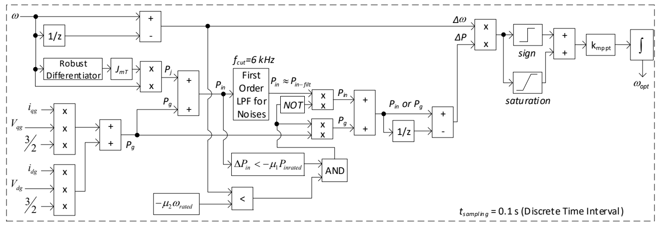

Fig. 6. The proposed inertial power-based HC for the MPPT control

Fortunately, the inertia does not have a significant variation depending on the operating conditions [47]. As seen in the scheme, the inertial power is calculated by the robust differentiator. Furthermore, the inertial power, P_j, is added to the generator power, P_g, and P_{in} along with ΔP_{in} are calculated from Eqs. (42) and (43), as shown in Fig. 6. Noises in P_{in} are filtered by a Low Pass Filter (LPF) to obtain the filtered power, $P_{in-filt}$. Consequently, the power equation is expressed as:

$$J_{mT}\omega\dot{\omega} = \omega T_{in} - \omega T_g \tag{42}$$

where $P_g = \omega T_g = 1.5\left(V_{dg}I_{dg} + V_{qg}I_{qg}\right)$ is the generator output power; $P_{in} = \omega T_{in}$ is the turbine input power, and $P_j = J_{mT}\omega\dot{\omega}$ is the inertial power. The small-signal linearized equation, in the transient for a sampling time, can be defined as:

$$\Delta P_{in} = \Delta P_g + \Delta P_j, \left(\Delta u = u_{(k)} - u_{(k-1)}\right), \left(u = P_{in}, P_g, P_j\right) \tag{43}$$

where k and $k-1$ are sample numbers. From Eq. (42), for large wind turbines, $P_{in} \approx P_g$ is valid in the steady state, since the generator speed is nearly constant. However, $P_{in} \approx P_j$ is valid in the transient, since $\dot{\omega} \gg 0$. From $P_{in} \approx P_j$ in the transient, $\Delta P_{in} \approx \Delta P_j$ is also valid in the transient. Since $\Delta P_{in}/\Delta\omega = 0$ is the real MPP, the inertial effect must be considered in the HC based MPPT control, as in the proposed HC. There are four situations for a fixed wind speed in the proposed HC based MPPT control. For fixed wind speed, by the control law given in Eq. (44), situations repeat the following order, $II \rightarrow I \rightarrow III \rightarrow IV$ [47]. These situations according to the proposed HC MPPT control rules are given as:

I. $\Delta\omega > 0$ & $\Delta P_{in} > 0$; so $\Delta P_{in}/\Delta\omega > 0$. This case means that P_{in} increases as ω increases. Thus, ω_{opt} is further increased to keep $\Delta\omega > 0$ & $\Delta P_{in} > 0$.

II. $\Delta\omega < 0$ & $\Delta P_{in} < 0$; so $\Delta P_{in}/\Delta\omega > 0$. In this case, P_{in} decreases as ω decreases. Thus, ω_{opt} is increased to ensure $\Delta\omega > 0$ & $\Delta P_{in} > 0$.

III. $\Delta\omega > 0$ & $\Delta P_{in} < 0$; so, $\Delta P_{in}/\Delta\omega < 0$. P_{in} decreases as ω increases, and thus, ω_{opt} is decreased to provide $\Delta\omega < 0$ & $\Delta P_{in} > 0$.

IV. $\Delta\omega < 0$ & $\Delta P_{in} > 0$; so, $\Delta P_{in}/\Delta\omega < 0$. P_{in} increases as ω decreases, and thus, ω_{opt} is further decreased to ensure $\Delta\omega < 0$ & $\Delta P_{in} > 0$.

This article has been accepted for publication in a future issue of this journal, but has not been fully edited. Content may change prior to final publication. Citation information: DOI 10.1109/TIE.2019.2907510, IEEE Transactions on Industrial Electronics

For a step variation of wind speed, only situations I and IV are triggered by the control law. For a positive slope ramp variation of the wind speed, $\Delta P_{in} > -\mu_1 P_{inrated}$ and $\Delta\omega > -\mu_1 \omega_{rated}$. Consequently, ω_{opt} is correctly increased by the control law of Eq. (44).

For a wind speed variation with a negative slope, if $\Delta P_{in} < -\mu_1 P_{inrated}$ and $\Delta\omega < -\mu_1 \omega_{rated}$. In this case, $\Delta P_g/\Delta\omega$ is evaluated instead of $\Delta P_{in}/\Delta\omega$, and thus ω_{opt} is correctly decreased by the control law of Eq. (44). These four rules and the conclusions above gives the proposed HC control law as:

$$\omega_{opt(k)} = \begin{cases} k_{mppt} \int_0^{t_{sampling}} \begin{pmatrix} sign\left(\Delta P_g \cdot \Delta\omega\right) \\ +sat\left(\Delta P_g \cdot \Delta\omega\right) \end{pmatrix} d\tau + \omega_{opt(k-1)} & if \begin{pmatrix} \Delta P_{in} < -\mu_1 P_{inrated} \\ \Delta\omega < -\mu_2 \omega_{rated} \end{pmatrix} \\ k_{mppt} \int_0^{t_{sampling}} \begin{pmatrix} sign\left(\Delta P_{in} \cdot \Delta\omega\right) \\ +sat\left(\Delta P_{in} \cdot \Delta\omega\right) \end{pmatrix} d\tau + \omega_{opt(k-1)} & if \begin{pmatrix} \Delta P_{in} > -\mu_1 P_{inrated} \\ \Delta\omega > -\mu_2 \omega_{rated} \end{pmatrix} \end{cases} \tag{44}$$

1) Avoiding Wrong Directionality in the Proposed HC

When situation I occurs, the wind speed increases suddenly, and hence T_{in} and P_{in} increases suddenly, and ω starts to increase in a ramp manner. The proposed HC can evaluate this increase in P_{in}. At a sampling interval (Δt), ω increases by $\Delta\omega$, and thus, the inertia stores much bigger amount of P_{in} during Δt due to increasing rotor speed. This leads to $\Delta P_g \approx 0$ and $\Delta P_{in} \approx \Delta P_j$, as explained before. The proposed HC considers the rate of change of the energy stored in the turbine inertia, P_j, and then calculates P_{in} by measuring P_g. P_j is calculated based on the robust differentiator given in the Section III. Consequently, P_j is added to P_g, and then $\Delta P_{in} > -\mu_1 P_{inrated}$ and $\Delta\omega > -\mu_1 \omega_{rated}$ are concluded. This causes the control law to start to increase ω_{opt}, as according to situation I. In other words, the control law does not trigger the other rules as in the conventional HC. This situation is verified by the experimental results in Figs. 10 and 11, as well.

Remark 4. Since the proposed HC processes and evaluates $\Delta P_{in}/\Delta\omega$ & $\Delta P_g/\Delta\omega$ while finding the MPP, it is not blind to wind speed changes. So, the problem of wrong directionality is eliminated.

2) Improved Performance of the Convergence Speed

P_{in} has two components, P_g and P_j. In the proposed HC, these components are separately measured and calculated, and then P_{in} is obtained by summing them. So, P_{in} has a smooth shape as expected. This enables to select a higher cut-off frequency f_{cut} values for the LPF, which filters the high frequency noises of P_{in}. Besides, it is possible select higher step sizes without causing the wrong directionality and oscillations around the MPP, since P_j is considered in the MPPT control. Therefore, the proposed inertial power-based HC solves the problems existed in the conventional HC. This performance is confirmed by the experimental results as shown in Figs. 10 and 11.

B. Conventional HC Method for the MPPT Control

The conventional HC, given in Fig. 5, is one of the simplest MPPT control algorithms that does not need a wind sensor and a priori knowledge of wind turbine. It evaluates the gradient of P_g with respect to ω, without considering the inertial effect, and the results are observed by continuously introducing a small perturbation to the control variable until the slope becomes zero. However, large perturbation step sizes increase the convergence speed but cause high amplitude oscillations around the MPP, which deteriorates the MPPT efficiency [47]. Small perturbation step sizes increase the MPPT efficiency, but slow the convergence speed, then a sluggish dynamical performance emerges. On selecting a step size, proven approaches are expert knowledge and trial and error methods [14], [15], [17], [18]. Besides, under rapid wind changes, there is a phenomenon called the wrong directionality [14], [47].

Remark 5. The conventional HC always evaluates $\Delta P_g/\Delta\omega$ in finding the MPP. So, it is blind to wind speed change since the inertial effect is neglected, and then the wrong directionality problem appears under rapid wind speed variations, which is caused by the non-minimum phase property in the generator output power [3]. This also leads to lower MPPT efficiency values, and unstable operation may happen [18]. These situations are explained and covered in many sources [14], [15].

The conventional HC control law is given in Eq. (45).

$$\omega_{opt(k)} = k_{mppt} \int_0^{t_{sampling}} sign\left(\Delta P_g \cdot \Delta\omega\right) dt + \omega_{opt(k-1)} \tag{45}$$

The conventional scheme considers $\Delta P_g/\Delta\omega = 0$ as seen from Eq. (45). $\Delta P_g/\Delta\omega = 0$ is the only MPP in the steady state, so the conventional HC cannot find the MPP in the transient with a high performance for small or large wind turbines.

1) Wrong Directionality Problem in the Conventional HC

Assuming that the wind speed increases, then P_{in} increases, and ω starts to increase, as well. This causes an increase in P_{in} according to situation I, but the conventional HC cannot evaluate this increase according the control law given in Eq. (45). After Δt, ΔP_g decreases, since the inertia absorbs P_{in} partly or completely. This leads to a sudden change in the sign of ΔP_g. Thus, $\Delta P_g < 0$ and $\omega > 0$ cause the algorithm jumps

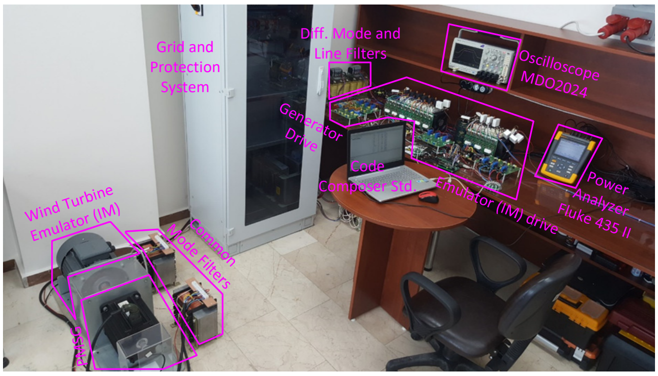

Fig. 7. Photo of the real experimental setup implemented in this work

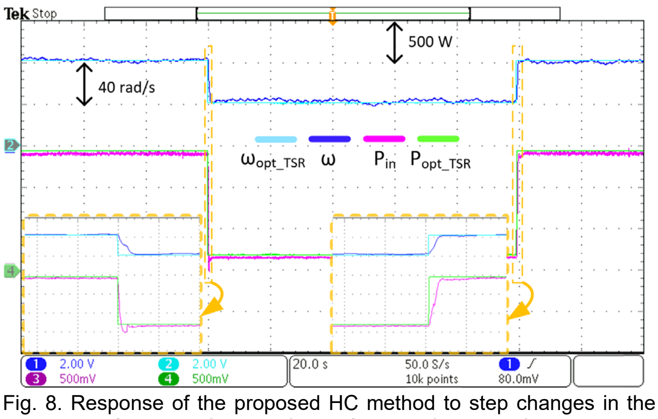

Fig. 8. Response of the proposed HC method to step changes in the wind speed from 10 m/s to 5 m/s and from 5 m/s to 10 m/s, and zooms

This article has been accepted for publication in a future issue of this journal, but has not been fully edited. Content may change prior to final publication. Citation information: DOI 10.1109/TIE.2019.2907510, IEEE Transactions on Industrial Electronics

to situation III, and therefore, ω_{opt} and ω begin to decrease. Decrement in ω causes the inertia to release the stored energy over the grid side converter to the grid. Thus, $\Delta P_g > 0$ and $\omega < 0$. This makes the algorithm jumps to situation IV. As ω_{opt} and ω decrease more and more, the power stored in the inertia is transferred to the grid more and more. Decrement in ω_{opt} and ω may continue up to zero, where the stored energy is totally depleted. Thus, this issue is called "wrong directionality under rapid wind change" [14], [47] since ω_{opt} is decreased instead of the fact that it is increased [15], [17].

2) Avoiding the Wrong Directionality in Conventional HC

If the step size is sufficiently smaller, the slope of the increasing and decreasing rotor speed becomes closer to zero. This avoids the wrong directionality but results in a sluggish dynamical performance of the convergence speed. For the conventional HC, there is a trade-off between the MPPT efficiency and the convergence speed. For these reasons, the conventional scheme is not feasible for wind turbines [17], [18], [47].

3) Low Performance Problem in the Conventional HC

P_g has two components, P_{in} and P_j. In the conventional HC, only P_g is measured. An LPF is needed to remove P_j from P_g to obtain P_{in}. So, this filter is not for noises but for extracting P_{in} from P_g [21]. Since P_j is a non-periodic time-varying signal under wind speed changes, an extremely low f_{cut} values for LPF should be selected. Such low f_{cut} values add a large phase shift to the control system, and consequently high amplitude oscillations around the MPP happens. Besides, large step sizes are another cause of the oscillations [21]. However, the LPF used in the proposed HC is for noises and relatively high f_{cut} values can be sufficient, and a trivial phase shift occurs [47].

V. Experimental Results and Discussion

The experimental set-up is shown in Figs. 2 (scheme) and 7 (photo), and all the parameters are given in Appendix. The dynamic performance of the proposed HC method is presented in Fig. 8 and compared with the TSR method for a wind speed profile with step-changes from 5 to 10 m/s and from 10 to 5 m/s. As seen in the figure, the convergence time is about 9.6 s and there is no wrong directionality. Furthermore, it is possible to see the high steady state performance. Fig. 9 shows the

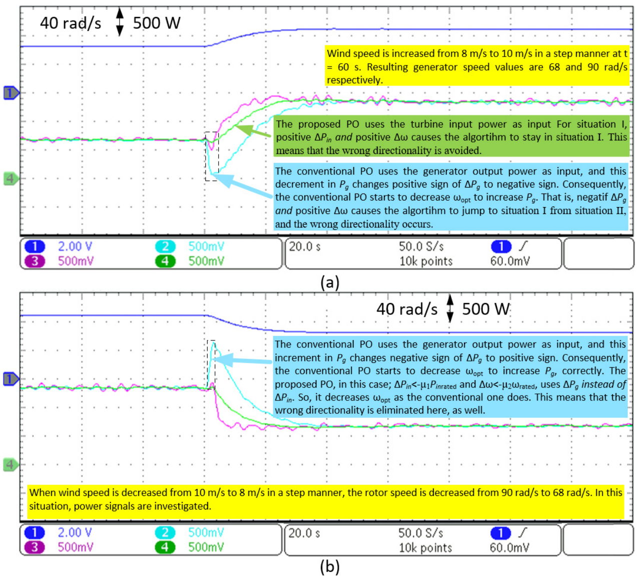

Fig. 9. (a) Speed and powers ($P_g, P_{in}, P_{in-filt}$) for a change in the wind speed from 8 m/s to 10 m/s; (b) from 10 m/s to 8 m/s

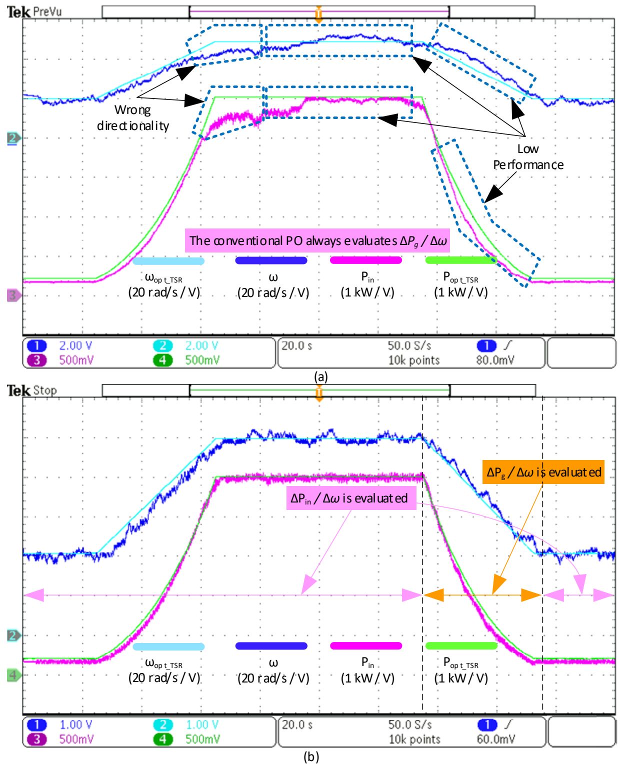

Fig. 10. Optimal and actual speeds, and turbine input power for a variable wind speed profile: (a) conventional HC method; and (b) proposed HC with the third order super-twisting sliding mode controllers

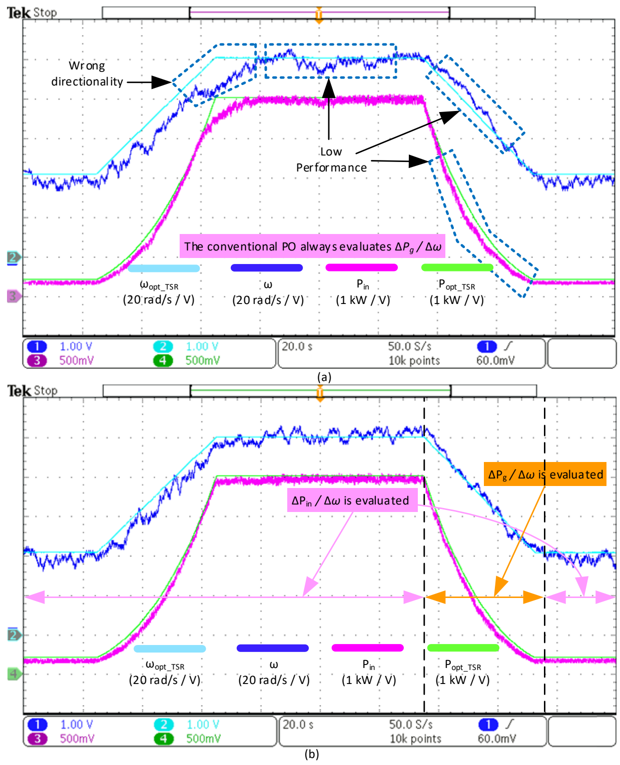

Fig. 11. Optimal and actual speeds, and turbine input power for a variable wind speed profile: (a) conventional HC method; and (b) proposed HC with the continuous integral sliding mode control

This article has been accepted for publication in a future issue of this journal, but has not been fully edited. Content may change prior to final publication. Citation information: DOI 10.1109/TIE.2019.2907510, IEEE Transactions on Industrial Electronics

response of the wind turbine for a wind speed of 8 m/s at t = 60 s, which increases to 10 m/s in (a) in a step manner. Later, it falls to 8 m/s at t = 60 s in (b) in a step manner. Fig. 9 reveals that P_g suddenly decreases from about 700 W to 100 W in 2 s, with an increment in the mechanical speed from 68 rad/s to 90 rad/s. It is because the inertia absorbs much amount of the turbine input power in the transient. Then it begins to increase and reaches 1375 W in about 38 s. As explained previously, the conventional HC algorithm causes the wrong directionality in this case. However, the proposed inertial power-based HC evaluates $\Delta P_{in}/\Delta\omega$, and $P_{in-filt}$ does not decrease at all with an increasing the rotor speed. Therefore, the wrong directionality is avoided by the proposed HC method. This implies that the trade-off existed in the conventional HC method is removed. Figs. 10 and 11 show ω_{opt_TSR} and P_{opt_TSR} obtained by the TSR method, and P_{in} is plotted for the proposed and conventional HC methods. A wind speed profile in a ramp manner is applied to the MPPT control system. In Figs. 10 and 11, the wrong directionality problem of the conventional HC method is highlighted for $\Delta P_{in} > 0$ and $\Delta\omega > 0$. It must be noted that there is no wrong directionality in the conventional HC for $\Delta P_{in} > 0$ and $\Delta\omega > 0$. For this reason, the proposed HC evaluates $\Delta P_{in}/\Delta\omega$ and $\Delta P_g/\Delta\omega$ in the cases of $\Delta P_{in} > -\mu_1 P_{inrated}$ & $\Delta\omega > -\mu_1\omega_{rated}$ and $\Delta P_{in} < -\mu_1 P_{inrated}$ & & $\Delta\omega < -\mu_1\omega_{rated}$, respectively, as observed from Figs. 10 and 11. As mentioned previously, the conventional HC cannot realize a precise MPP detection in the transient. This low performance is also indicated in Figs. 10 and 11 either in the transient or in the steady state. However, the proposed inertial power-based HC yields a more precise MPP detection than the conventional one. The total energy captured from the wind, with TOSSMC, is 265,3 kWs by the proposed HC, while it is 232.8 kWs by the conventional HC. The total energy harvested from the wind is, with CISMC, 258,7 kWs by the proposed HC, while it is 234.1 kWs by the conventional HC. Consequently, there is an increase in the captured energy, thanks to the proposed HC, by 13.96 % with TOSSMC, and by 10.51 % with CISMC. The MPPT efficiency of the proposed HC method is 95.08 % for TOSSMC and 92.71 % for CISMC. The MPPT efficiency of the conventional one is 83.43 % for TOSSMC and 83.9 % for CISMC. It must be noted that CISMC causes more chattering in the control input than TOSSMC as seen from Figs. 10 and 11.

Finally, it is worth noting that experiments performed with the rated wind speed showed that the total harmonic distortions of generator and grid currents are below 4.0 %, within the level recommended by grid codes. Furthermore, the power factor of the grid side converter is 0.99, remarkably close to 1.0.

VI. Conclusion

The aim of this study was to avoid that the energy stored in the inertia of the wind rotor affects the MPPT performance, and in this context, a new HC MPPT method was proposed. So, this means that the inertial effect is compensated by the proposed HC method. Besides, to track the MPP generated by the proposed HC, third order super-twisting and continuous integral sliding mode controllers are designed and applied to the control of the generator and grid side converters. Thanks to the proposed HC method, the wrong directionality problem of the conventional HC was overcome by considering the inertial energy. Furthermore, the use of low f_{cut} values in the conventional HC were avoided in the proposed HC. For these reasons, the proposed HC yielded higher convergence speed than the conventional one. That is, the MPPT efficiency was improved by accurately finding the MPP with a high performance either in the transient or in the steady state. The proposed inertial power-based HC provided an increase in the captured power from the wind about 13.96 % and an increase in the MPPT efficiency about 11.65 % for TOSSMC. For CISMC, the increases in the captured power and in the MPPT efficiency are 10.51 % and 8.81 %, respectively. The proposed MPPT control system employed only one parameter as a priori, the total turbine inertia at the generator side. As in the conventional one, the proposed HC did not need a wind sensor, as well. The sliding mode controllers made it possible that the MPP can be precisely tracked by the generator. The control of generator as well as grid side converter for a high-performance tracking of the MPP were performed using third order super-twisting and continuous sliding mode controllers. It is concluded that the TOSSMC possesses less chattering than the CISMC. In this regard, by TOSSMC, more energy is harvested from the wind. In the following table, the comparison results are presented for the proposed and conventional HC searching MPPT control methods.

TABLE 1. PERFORMANCE COMPARISON

Performance Criterion	Proposed HC MPPT Control	Conventional HC MPPT Control
Wrong directionality	Not appear	It occurs for a wind speed variation with positive slope
Tracking of MPP for a positive slope wind speed variation	With high performance	Not possible because of the wrong directionality
Tracking of MPP for a negative slope wind speed variation	With high performance	Unacceptable performance because of neglected inertial effect
Steady state MPP speed error	Below 2.88 %	11.2 % speed error
$MPPT\ efficiency$ (%) $= W_{in}/W_{opt\_TSR}$	95.08 % with TOSSMC 92.71 % with CISMC	83.43 % with TOSSMC 83.9 % with CISMC
Captured energy from the wind, W_{in}	265.3 kWs with TOSSMC 258.7 kWs with CISMS	232.8 kWs with TOSSMC 234.1 kWs with CISMS

Appendix

A. Parameters and Rated Values

TABLE 2. WIND TURBINE PARAMETERS

Parameter	Notation	Value
Rated turbine input power	$P_{inrated}$	2.5 kW
Air density, Turbine radius	ρ, R	1.14 kg/m^3, 1.3 m
C_p coefficients	C_1, C_2, C_3, C_4, C_5, C_6	0.5176, 116, 0.4, 5, 21, 0.0068
Rated wind speed	V_{rated}	12 m/s
Optimal power coefficient	C_{pmax}	0.48
Wind rotor inertia	J_r	10 kg/m^2
Gear ratio	-	3/4
Rated wind rotor speed	ω_{rrated}	75 rad/s

TABLE 3. POWER CONVERTER PARAMETERS

Parameter	Notation	Value

This article has been accepted for publication in a future issue of this journal, but has not been fully edited. Content may change prior to final publication. Citation information: DOI 10.1109/TIE.2019.2907510, IEEE Transactions on Industrial Electronics

Line filter for grid side converter	R_d, L_d	0.25 Ω, 2.3 mH
Common mode filter	L_c	15 mH
DC bus capacitor	C_{dc}	3400uF
Grid phase voltages	V_{as}, V_{bs}, V_{cs}	110 Vrms, 50 Hz
DC bus voltage	V_{dc}	400V
IGBT driver	*SEMIKRON*	Skyper 32 PRO R
IGBT module	*SEMIKRON*	SKM150GB12T4
Current and voltage sensors	*LEM*	LA55-P and LV25-P
Diode module	*SEMIKRON*	SKKD100/12
Heatsink	*SEMIKRON*	0.12K/W

TABLE 4. INDUCTION MOTOR PARAMETERS

Parameter	Notation	Value
Rotor phase resistance	R_r	3 Ω
Stator phase resistance	R_s	2.355 Ω
Stator phase leakage inductance	L_{ss}	0.0162 H
Rotor phase leakage inductance	L_{rr}	0.0162 H
Magnetizing inductance	L_m	0.4286 H
Rated values	*IM*	5.5 kW, 2 poles, 400 V, 11 A, 1455 rpm, 36 Nm
Rotor reference flux	λ_{dr_ref}	1.0715 Wb
Motor inertia	J_m	0.026 kgm^2
Torque constant	k_t	3.09 Nm/A

TABLE 5. GENERATOR PARAMETERS

Parameter	Notation	Value
Stator phase resistance	R_s	0.25 Ω
Stator phase inductance	L_s	L_{qg}=3.2 mH, L_{dg}=1.7 mH
Rotor magnetizing flux	λ_m	0.21 Wb
Rated values	*PMSG*	5 kW, 4 poles, 400 V, 15 A, 2000 rpm, 24 Nm
Generator inertia	J_g	0.00657 kgm^2
Torque constant	k_t	1.26 Nm/A

TABLE 6. CONTROL PARAMETERS

Parameter	Notation and Value
Third order sliding mode controller	k_1=110, k_2=0.0012, k_3=1045, k_4=104, k_5=0.0013, k_6=1055
Second order sliding mode controller	α=78, β=787
Rob. Diff. for third order sliding mode controllers	$\alpha_1=\alpha_3=76$, $\beta_1=\beta_3=183$
Rob. Diff. for proposed HC	α=43, β=132
Parameters for proposed HC	k_{mppt}=4,0, μ_1=0.0036, μ_2=0.0001 $sat = \pm 2.2$
Parameters of continuous integral sliding mode controller	k_7=1.5, k_8=0.8, k_9=1.3, k_{10}=0.65, $\eta_1=91$, $\eta_2=970$, $\eta_3=88$, $\eta_4=890$

B. Proof of the Inertial Effect Compensation in the Proposed HC MPPT Method

Fig. 12 shows two different situations for a wind speed variation (wind speed variation with positive and negative slope) used to explain how the proposed HC MPPT control is not affected by the inertial response. It was obtained by TSR based MPPT control with the exact model knowledge.

1) Wind Speed Variation with Positive Slope

Conventional HC: With an increase in the wind speed, Transient 1 occurs. Then, the turbine inertia stores some portion of the input power according to the largeness of the inertia and slope of the turbine speed variation, which causes a decrease in the generator output power. According to the control law given in Eq. (45), the conventional HC starts to decrease the turbine speed. This is the wrong directionality, since the turbine speed needs to be increased towards the MPPT point *b*. Decreasing the turbine speed results in that the stored energy is released to the grid, which causes an increase in the generator output power due to the inertial response. So, the conventional HC continues decreasing the turbine speed until the rate of change of stored energy does not supply a power higher than the wind does. The MPPT performance of the conventional HC is low because of the wrong directionality or the inertial response.

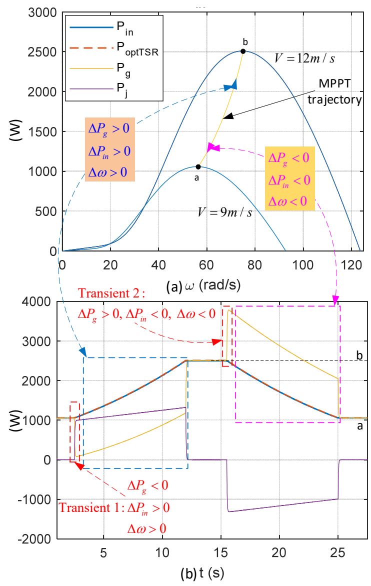

Fig. 12. (a) MPPT trajectory; and (b) power vs. time for a wind speed variation between 9 and 12 m/s

Proposed HC: The proposed HC also calculates the turbine input power. As in the previous situation, during Transient 1, the proposed HC correctly starts to increase the turbine speed towards the MPPT point *b* according to the control law given in Eq. (44), since it uses the turbine input power as input. There is no wrong directionality, and the inertial response does not affect the proposed HC based MPPT control.

2) Wind Speed Variation with Negative Slope

Conventional HC: With a decrease in the wind speed, Transient 2 occurs. During Transient 2, the turbine inertia releases some portion of the input power, and this causes an increase in the generator output power. According to the control law given in Eq. (45), the conventional HC correctly starts to decrease the turbine speed towards the MPPT point *a*, this means that no wrong directionality happens.

Proposed HC: According to the control law given in Eq. (44), the wind speed variation with negative slope enables the proposed HC to employ the generator output power instead of the turbine input power as input. Thus, the turbine speed is driven to the MPPT point *a* correctly, just as in the conventional HC, without a wrong directionality.

REFERENCES

[1] K. Tan, and S. Islam, “Optimum control strategies in energy conversion of PMSG wind turbine system without mechanical sensors,” *IEEE Transactions on Energy Conversion*, vol. 19, no. 2, pp. 392-399, Jun. 2004.

[2] V. Yaramasu and B. Wu. *Model Predictive Control of Wind Energy Conversion Systems,* John Wiley & Sons, Inc., Hoboken, NJ, USA, 2017.

[3] M. Nasiri, J. Milimonfared, S. H. Fathi, “Modeling, analysis and comparison of TSR and OTC methods for MPPT and power smoothing in permanent magnet synchronous generator-based wind turbines” *Energy Conversion and Management*, vol. 86, pp. 892-900, June 2014.

[4] D. M. Abdullah, A. Yatim, C. Tan, and R. Saidur, “A review of maximum power point tracking algorithms for wind energy systems,” *Renewable and Sustainable Energy Reviews*, vol. 16, no. 5, pp. 3220–3227, 2012.

[5] Z. Chen, M. Yin, Y. Zou, K. Meng and Z. Dong, "Maximum Wind Energy Extraction for Variable Speed Wind Turbines with Slow Dynamic Behavior," *IEEE Transactions on Power Systems*, vol. 32, no. 4, pp. 3321-3322, July 2017.

[6] Q. Wang and L. Chang, "An intelligent maximum power extraction algorithm for inverter-based variable speed wind turbine systems," *IEEE Transactions on Power Electronics*, vol. 19, no. 5, pp. 1242-1249, Sept. 2004.

[7] R. Aubrée, F. Auger, M. Macé, and L. Loron, "Design of an efficient small wind-energy conversion system with an adaptive sensorless MPPT strategy", *Renewable Energy*, vol. 86, pp. 280-291, Feb. 2016.

[8] C. Tang, M. Pathmanathan, W. L. Soong, and N. Ertugrul, "Effects of inertia on dynamic performance of wind turbines," in *2008 Australas. Univ. Power Eng. Conf.*, Sydney, NSW, Australia, 2008, pp. 1-6.

[9] E. Koutroulis and K. Kalaitzakis, "Design of a maximum power tracking system for wind-energy-conversion applications," *IEEE Trans. Ind. Electron.*, vol. 53, no. 2, pp. 486–494, Apr. 2006.

[10] R. J. Wai and C. Y. Lin, "Implementation of Novel Maximum-Power-Extraction Algorithm for PMSG Wind Generation System without Mechanical Sensors," in *2006 IEEE Conference on Robotics, Automation and Mechatronics*, Bangkok, Thailand, 2006, pp. 1-6.

[11] S. A. M. Saleh, "Testing the Performance of a Resolution-Level MPPT Controller for PMG-Based Wind Energy Conversion Systems," *IEEE Transactions on Industry Applications*, vol. 53, no. 3, pp. 2526-2540, May-June 2017.

[12] S. M. R. Kazmi, H. Goto, H. J. Guo and O. Ichinokura, "A Novel Algorithm for Fast and Efficient Speed-Sensorless Maximum Power Point Tracking in Wind Energy Conversion Systems," *IEEE Transactions on Industrial Electronics*, vol. 58, no. 1, pp. 29-36, Jan. 2011.

[13] H. Fathabadi, "Novel Maximum Electrical and Mechanical Power Tracking Controllers for Wind Energy Conversion Systems," *IEEE Journal of Emerging and Selected Topics in Power Electronics*, vol. 5, no. 4, pp. 1739-1745, Dec. 2017.

[14] S. Lalouni, D. Rekioua, K. Idjdarene and A. Tounzi, "Maximum Power Point Tracking Based Hybrid Hill-climb Search Method Applied to Wind Energy Conversion System," *Electric Power Components and Systems*, vol. 43, no. 8-10, pp. 1028-1038, 2015.

[15] R. M. Linus and P. Damodharan, "Maximum power point tracking method using a modified perturb and observe algorithm for grid connected wind energy conversion systems," *IET Renewable Power Generation*, vol. 9, no. 6, pp. 682-689, 2015.

[16] K. H. Kim, T. L. Van, D C. Lee, S. H. Song, and E. H. Kim, "Maximum output power tracking control in variable-speed wind turbine systems considering rotor inertial power," *IEEE Trans. Ind. Electron.,* vol. 60, no. 8, pp. 3207–3217, Aug. 2013.

[17] R. I. Putri, M. Pujiantara, A. Priyadi, T. Ise and M. H. Purnomo, "Maximum power extraction improvement using sensorless controller based on adaptive perturb and observe algorithm for PMSG wind turbine application," *IET Electric Power Applications*, vol. 12, no. 4, 2018.

[18] Z. M. Dalala, Z. U. Zahid, W. Yu, Y. Cho and J. S. Lai, "Design and Analysis of an MPPT Technique for Small-Scale Wind Energy Conversion Systems," *IEEE Transactions on Energy Conversion*, vol. 28, no. 3, pp. 756-767, Sept. 2013.

[19] R. M. Linus and P. Damodharan, "Wind Velocity Sensorless Maximum Power Point Tracking Algorithm in Grid-connected Wind Energy Conversion System," *Electric Power Components and Systems*, vol. 43, no. 15, pp. 1761-1770, 2015.

[20] C. T. Pan and Y. L. Juan, "A Novel Sensorless MPPT Controller for a High-Efficiency Microscale Wind Power Generation System," *IEEE Trans. on Energy Conversion*, vol. 25, no. 1, pp. 207-216, March 2010.

[21] M. Narayana, G.A. Putrus, M. Jovanovic, P.S. Leung, and S. McDonald, "Generic maximum power point tracking controller for small-scale wind turbines," *Renewable Energy*, vol. 44, pp. 72-79, Aug. 2012.

[22] M. Karabacak and H. I. Eskikurt, "Speed and current regulation of a permanent magnet synchronous motor via nonlinear and adaptive backstepping control," *Mathematical and Computer Modelling*, vol. 53, no. 9–10, pp. 2015-2030, May. 2011.

[23] M. Karabacak and H. I. Eskikurt, "Design, modelling and simulation of a new nonlinear and full adaptive backstepping speed tracking controller for uncertain PMSM," *Applied Mathematical Modelling*, vol. 36, no. 11, pp. 5199-5213, Nov. 2012.

[24] B. Yang, T. Yu, H. Shu, J. Dong, and L. Jiang, "Robust sliding-mode control of wind energy conversion systems for optimal power extraction via nonlinear perturbation observers," *Applied Energy*, vol. 210, pp. 711-723, 15 Jan. 2018.

[25] W.-M. Lin and C.-M. Hong, "Intelligent approach to maximum power point tracking control strategy for variable-speed wind turbine generation system," *Energy*, vol. 35, no. 6, pp. 2440-2447, Jun. 2010.

[26] X.-X. Yin, Y.-G. Lin, W. Li, Y.-J. Gu, H.-W. Liu, and P.-F. Lei, "A novel fuzzy integral sliding mode current control strategy for maximizing wind power extraction and eliminating voltage harmonics," *Energy*, vol. 85, pp. 677-686, 1 Jun. 2015.

[27] K. Belmokhtar, M. L. Doumbia, and K. Agbossou, "Novel fuzzy logic based sensorless maximum power point tracking strategy for wind turbine systems driven DFIG (doubly-fed induction generator)", *Energy*, vol. 76, pp. 679-693, 1 Nov. 2014.

[28] F. Jaramillo-Lopez, G. Kenne, and F. Lamnabhi-Lagarrigue, "A novel online training neural network-based algorithm for wind speed estimation and adaptive control of PMSG wind turbine system for maximum power extraction," *Renewable Energy*, vol. 86, pp. 38-48, Feb. 2016.

[29] X. Liu, Y. Han and C. Wang, "Second-order sliding mode control for power optimisation of DFIG-based variable speed wind turbine," *IET Renewable Power Generation*, vol. 11, no. 2, pp. 408-418, 2 8 2017.

[30] M. I. Martinez, A. Susperregui and G. Tapia, "Second-order sliding-mode-based global control scheme for wind turbine-driven DFIGs subject to unbalanced and distorted grid voltage," *IET Electric Power Applications*, vol. 11, no. 6, pp. 1013-1022, 7 2017.

[31] B. Beltran, M. E. H. Benbouzid and T. Ahmed-Ali, "Second-Order Sliding Mode Control of a Doubly Fed Induction Generator Driven Wind Turbine," *IEEE Transactions on Energy Conversion*, vol. 27, no. 2, pp. 261-269, Jun. 2012.

[32] B. Beltran, T. Ahmed-Ali and M. E. H. Benbouzid, "High-Order Sliding-Mode Control of Variable-Speed Wind Turbines," *IEEE Transactions on Industrial Electronics*, vol. 56, no. 9, pp. 3314-3321, Sep. 2009.

[33] S. Kamal and B. Bandyopadhyay, "Higher Order Sliding Mode Control: A Control Lyapunov Function Based Approach," *WSEAS Trans. Syst. Control*, vol. 9, pp. 38–46, 2014.

[34] C. Evangelista, P. Puleston, F. Valenciaga, and L. M. Fridman, "Lyapunov-Designed Super-Twisting Sliding Mode Control for Wind Energy Conversion Optimization," *IEEE Trans. Ind. Electron.*, vol. 60, no. 2, pp. 538–545, Feb. 2013.

[35] F. Kreith, *Principles of Sustainable Energy Systems*, CRC Press, 2010.

[36] N. P. Quang, and J. A. Dittrich, *Vector Control of Three-Phase AC Machines System Development in the Practice*, Springer, Berlin, 2015.

[37] S. Kamal, A. Chalanga, J. A. Moreno, L. Fridman and B. Bandyopadhyay, "Higher order super-twisting algorithm," in *2014 13th International Workshop on Variable Structure Systems (VSS)*, Nantes, 2014, pp. 1-5.

[38] A. Chalanga, S. Kamal, L. M. Fridman, B. Bandyopadhyay and J. A. Moreno, "Implementation of Super-Twisting Control: Super-Twisting and Higher Order Sliding-Mode Observer-Based Approaches," *IEEE Trans. Industrial Electronics*, vol. 63, no. 6, pp. 3677-3685, Jun. 2016.

[39] X. Yu and M. Ö Efe, *Recent Advances in Sliding Modes: From Control to Intelligent Mechatronics*, Springer, 2015.

[40] N. Mohan, *Advanced Electric Drives: Analysis, Control, and Modeling Using MATLAB/Simulink*, John Wiley & Sons, 2014.

[41] S. Kamal, J. A. Moreno, A. Chalanga, B. Bandyopadhyay, and L. M. Fridman, "Continuous terminal sliding-mode controller," *Automatica*, vol. 69, pp. 308-314, Jul. 2016.

[42] M. Karabacak, "A Novel Nonlinear and Adaptive Control of Grid Connected Inverters," J. Circuit. Syst. Comp., vol. 25, no. 11, 2016.

[43] J. Dannehl, C. Wessels and F. W. Fuchs, "Limitations of Voltage-Oriented PI Current Control of Grid-Connected PWM Rectifiers with LCL Filters," *IEEE Transactions on Industrial Electronics*, vol. 56, no. 2, pp. 380-388, Feb. 2009.

[44] Y. Shtessel, M. Taleb, and F. Plestan, "A novel adaptive-gain supertwisting sliding mode controller: Methodology and application," *Automatica*, vol. 48, no. 5, pp. 759-769, May. 2012.

[45] A. Levant, "Robust exact differentiation via sliding mode technique," *Automatica*, vol.34, no. 3, pp. 379-384, 1 Mar. 1998.

[46] A. Chalanga, S. Kamal and B. Bandyopadhyay, "A New Algorithm for Continuous Sliding Mode Control with Implementation to Industrial Emulator Setup," in IEEE/ASME Transactions on Mechatronics, vol. 20, no. 5, pp. 2194-2204, Oct. 2015.

[47] M. Karabacak, "A New Perturb and Observe Based Higher Order Sliding Mode MPPT Control of Wind Turbines Eliminating the Rotor Inertial Effect," Renewable Energy, vol. 133, pp. 807-827, April 2019.

Murat Karabacak received the B.Sc. degree from Kocaeli University, Kocaeli, Turkey, in 2004, and the M.Sc. degree from Duzce University, Duzce, Turkey, in 2008, and the Ph.D. degree from Sakarya University,

Sakarya, Turkey, in 2012. From 2007 to 2012, he had been with Duzce University, Duzce. In 2012, he joined Sakarya University as an Assistant Professor with the Department of Electrical and Electronics Engineering. In 2018, he joined Sakarya University of Applied Sciences, where he is currently an Associate Professor with the Department of Electrical and Electronics Engineering and the Head of the Power Electronics Technologies and Renewable Energy Systems Research Lab. His research interests include power converters, electric drives, wind and solar photovoltaic energy systems, adaptive control, sliding mode control, and microgrids.

Luis M. Fernández-Ramírez (M’11–SM’15) was born in Los Barrios, Cadiz, Spain. He received the M.Sc. degree in electrical engineering from the University of Seville, Seville, Spain, in 1997, and the Ph.D. degree from the University of Cadiz, Cadiz, Spain, in 2004.
From 1997 to 2000, he was with the Department of Development and Research, Desarrollos Eolicos S.A., Seville. In 2000, he joined the University of Cadiz, where he is currently an Associate Professor with the Department of Electrical Engineering and the Head of the Research Group in Electrical Technologies for Sustainable and Renewable Energy (PAIDI-TEP023). His current research interests include renewable energy sources, energy storage systems, hydrogen and fuel cell systems, electric vehicles, smart grids, power converters and energy management/control systems.

Tariq Kamal (S’15) received the M.Sc. degree in electrical engineering from COMSATS university, Islamabad, Pakistan in 2015. Currently, he is a Ph.D. student in energy and sustainability engineering at the University of Cadiz, Spain; and in electrical power engineering at the Sakarya University, Turkey. His research interests include advanced intelligent control techniques to power systems; modern power electronics; modelling, control, and analysis of power systems; hybrid renewable energy systems (solar photovoltaic, wind, fuel cells, hydro including microgrid design, power management and power market); and the application of signal processing (wavelets, B-spline functions) in power systems. He is the author/co-author of more than 50 papers published in various international scientific journals and IEEE/SpringerNature peer-reviewed conferences and proceedings.

Shyam Kamal (M’19) received his bachelor’s degree in Electronics and Communication Engineering from the Gurukula Kangri Vishwavidyalaya Haridwar, Uttrakhand, India in 2009, and Ph.D. in Systems and Control Engineering from the Indian Institute of Technology Bombay, India in 2014. From 2014 to 2016, he was with the Department of Systems Design and Informatics, Kyushu Institute of Technology. Currently, he is an Assistant Professor in Department of Electrical Engineering, Indian Institute of Technology (BHU) Varanasi, India. He has published one monograph and 57 journal articles and conference papers. His research interests include the areas of fractional order systems, contraction analysis, discrete and continuous higher order sliding mode control.